Journal of Biomechanical Science and Engineering

Vol. 4, No. 1, 2009

A Numerical Analysis of Dynamic Flight Stability of Hawkmoth Hovering*

Na GAO**, Hikaru AONO*** and Hao LIU**

**Graduate School of Engineering, Chiba University

1-33, Yayoi-cho, Inage-ku, Chiba

E-mail: hliu@faculty.chiba-u.jp

***Department of Aerospace Engineering, University of Michigan

Ann Arbor, MI 48109 USA 734-764-1817

Abstract

A numerical analysis of dynamic flight stability of a hovering hawkmoth is presented. A computational fluid dynamic (CFD) method is used to simulate the unsteady flow about a realistic hawkmoth model and to compute the aerodynamic derivatives of the aerodynamic forces and pitching moment in response with a series of small disturbances. With these parameters, the techniques of eigenvalue and eigenvector analysis is employed to investigate dynamic flight stability of the hawkmoth hovering. In the longitudinal disturbance motion, three natural modes are identified of a stable oscillatory mode, a stable fast subsidence mode and a stable slow subsidence mode, which indicate that the hawkmoth hovering flight is stable. In short, a hovering hawkmoth, if the body motion is dynamically stable and hence the disturbance dies out fast, might not need to make any adjustment with wing motions and could return to the equilibrium state 'automatically'.

Key words: CFD, Dynamic Flight Stability, Hovering, Hawkmoth, Natural Modes of Motion

1. Introduction

Recently, in response to increasing requirement on the research and development of micro air vehicles (MAVs), studies on aerodynamics of insect and bird flights have been taken more and more attention by biologists, mathematicians, and engineers, etc. In the past decades, much work has been done on uncovering novel aerodynamic mechanisms in insect flights and remarkable progress has been achieved both experimentally and numerically. On the other hands, there are still comparatively few studies on dynamic stability of insect flight, which are no doubt of great importance in understanding insect flapping flight and in providing novel mechanisms for the MAV design as well.

Thomas and Taylor[1] and Taylor and Thomas[2] for the first time performed two static stability analysis of the gliding flight and the flapping flight. They approached the problem by analyzing the stability of a flapping wing by means of the quasi-static assumption and the blade element methods. They found that flapping flight is not inherently destabilizing, but can in fact enhance stability if the mean quasi-static flight force acts in an appropriate place. Furthermore, Taylor and Thomas[3] studied dynamic flight stability of the desert locust *Schistocerca gregaria*. They used a classical linearized framework borrowed directly from the aircraft flight literature to analyze force measurements from tethered locusts. Using the techniques of eigenvalue and eigenvector, they studied the longitudinal dynamic flight stability of a forward flight locust. The study provided the first formal quantitative analysis of dynamic stability in a flying animal. More recently, Sun and Xiong[4] studied

*Received 7 May, 2008 (No. 08-0352)
[DOI: 10.1299/jbse.4.105]

longitudinal dynamic flight stability of a hovering bumblebee by means of the same analysis approach, but they calculated the aerodynamic forces and moments using the method of computational fluid dynamics (CFD). They represented the natural modes from a longitudinal disturbed motion of the desert locust and bumblebee. They concluded that flapping flight didn't have any inherently destabilizing effect: beating the wing faster didn't induce the disturbance but can enhance the existing stability or instability.

In the present paper, by means of an insect dynamic flight simulator it is able to mimic realistic flapping flights of insects and to provide quantitative prediction on aerodynamics and energetics associated with insect flights [5, 6, 7, 8]. We present, for the first time, an analysis of the longitudinal dynamic stability in a hovering hawkmoth. The morphological and kinematic models employed in this study are constructed realistically based on those by Aono and Liu[7], and by Willmott and Ellington[9]. In modeling the longitudinal dynamic stability, we also consider the insect body as rigid; the "quasi-steady" approximation is used and the linearized equation of motion is hereby solved.

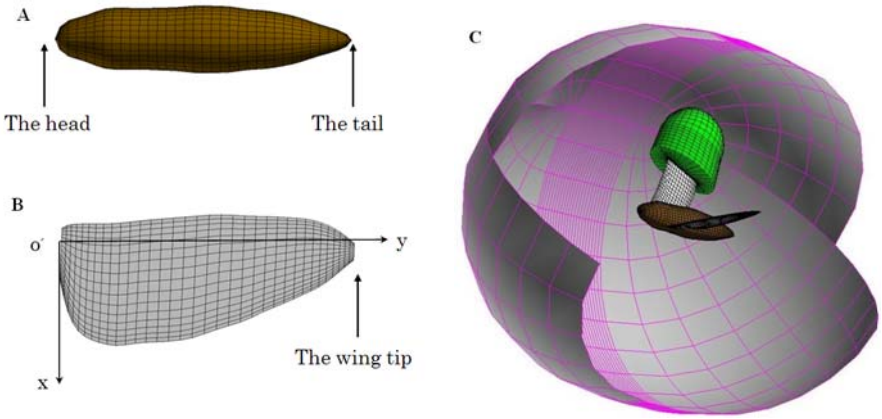

Fig. 1. Grid systems of the body (A), the wing (B), and the wing-body moth model (C).

2. Materials and methods

2.1 A dynamic flight simulator

In the study by Taylor and Thomas[3], the conventional methods by measuring the aerodynamic derivatives of the aircraft, helicopters and airships in the wind tunnel were extended to the dynamic stability analysis of insect flight. Accurately measuring the aerodynamic forces and their derivatives associated with a real insect in flapping flight, however, is tough and difficult. Comparatively, it may be more straightforward and easily handful to use the CFD methods to predict those aerodynamic derivatives, and hence a dynamic flight simulator is employed in the present study [6, 7, 8].

2.1.1 Geometrical and kinematic model of a hovering hawkmoth

As shown in Fig. 1, the grid systems utilized in the present study are composed of three structured grid systems (one global grid for the body system and two local ones for the wings). The body block consists of 45×45×95 grids and the single wing block of 45×45×31 grids.

The kinematic modeling of the flapping wings and the body is based on the realistic kinematics of a hovering hawkmoth in terms of the stroke plane angle and the body angle in defining the body attitude and the three basic motions of the flapping wing. The flapping wing consists of three basic motions as depicted in Fig. 2: (1) flapping in the stroke plane by the positional angle (ϕ); (2) rotation of wing, about the z-axis, out of the stroke plane on either side described by the elevation angle (θ); and (3) feathering of the wing with respect to the stroke plane by varying the angle of attack of the wing (α). The time-varying positional angle, elevation angle and angle of attack of the wing (or feathering angle) are defined by using the first three Fourier terms as:

$$\phi(t) = \sum_{n=0}^{3} [\phi_{cn} \cos(nKt) + \phi_{sn} \sin(nKt)] \quad (1)$$

$$\theta(t) = \sum_{n=0}^{3} [\theta_{cn} \cos(nKt) + \theta_{sn} \sin(nKt)] \quad (2)$$

$$\alpha(t) = \sum_{n=0}^{3} [\alpha_{cn} \cos(nKt) + \alpha_{sn} \sin(nKt)] \quad (3)$$

Note that K is the reduced frequency defined as, $2\pi fc_m/(2U_{ref})$, where f is the wingbeat frequency, c_m is a reference length of the mean wing chord length and U_{ref} is a reference velocity of the mean velocity at wing tip. And the coefficients ϕ_{cn}, ϕ_{sn}, θ_{cn}, θ_{sn}, α_{cn}, and α_{sn} are determined from the empirical kinematic data[7, 9].

2.1.2 Solutions to the Navier-stokes equation

The governing equations are the three-dimensional, incompressible, unsteady Navier-Stokes equations written in a strong conservation form for mass and momentum, and nondimensionalized in an integral form, written as:

$$\int_{V(t)} \frac{\partial \mathbf{q}}{\partial \tau} dV + \frac{\partial}{\partial t} \int_{V(t)} \mathbf{Q} dV + \oint_{S(t)} (\mathbf{f} - \mathbf{Q}\mathbf{u}_g) \cdot \mathbf{n} dS = 0 \quad (4)$$

where the last term $\mathbf{f} = (\mathbf{F}+\mathbf{F}_v, \mathbf{G}+\mathbf{G}_v, \mathbf{H}+\mathbf{H}_v)$ represents the net flux across the cell surfaces. Other terms are defined as

$$\mathbf{Q} = \begin{bmatrix} u' \\ v' \\ w' \\ 0 \end{bmatrix}, \quad \mathbf{q} = \begin{bmatrix} u' \\ v' \\ w' \\ p \end{bmatrix}, \quad \mathbf{F} = \begin{bmatrix} u'^2 + p \\ u'v' \\ u'w' \\ \beta u' \end{bmatrix}, \quad \mathbf{G} = \begin{bmatrix} v'u' \\ v'^2 + p \\ v'w' \\ \beta v' \end{bmatrix}, \quad \mathbf{H} = \begin{bmatrix} w'u' \\ w'v' \\ w'^2 + p \\ \beta w' \end{bmatrix}$$

$$\mathbf{F}_V = -\left(\frac{1}{Re} + \upsilon_t\right) \begin{bmatrix} 2u'_x \\ u'_y + v'_x \\ u'_z + w'_x \\ 0 \end{bmatrix}, \mathbf{G}_V = -\left(\frac{1}{Re} + \upsilon_t\right) \begin{bmatrix} u'_y + v'_x \\ v'_y \\ v'_z + w'_y \\ 0 \end{bmatrix}, \mathbf{H}_V - \left(\frac{1}{Re} + \upsilon_t\right) \begin{bmatrix} w'_x + u'_z \\ v'_z + w'_y \\ 2w'_z \\ 0 \end{bmatrix}$$

In the preceding equations, β is the pseudo-compressibility coefficient; p is pressure; u',v' and w' are the x-, y- and z- components of velocity in Cartesian coordinate system; t denotes physical time while τ is pseudo time; and Re is the Reynolds number. Note that the term q associated with the pseudo time is designed for an inner-iteration at each physical time step, and will vanish when the divergence of velocity is driven to zero so as to satisfy the equation of continuity. More details can be found in Liu and Kawachi[5], Aono and Liu[7] and Aono et al.[8].

2.2 Linearized equations of motion of a hovering hawkmoth

Follow Taylor and Thomas[3] the 'rigid body' assumption is employed here that an insect has only 6 degrees of freedom (DOF) of a rigid body and the effects of the flapping wings on the flight system can be represented by wingbeat-cycle-average aerodynamic and inertial forces and moments that vary with time over the time scale of the insect body. Furthermore, the animal's motion is assumed to consist of small disturbances from the equilibrium condition; and thus the linear theory of aircraft flight dynamics is applicable to the analysis of insect flight dynamics. On the basis of the simplified or linearized equations of motion, the longitudinal dynamic flight stability of insect hovering can be considered with 3 DOF: the forward, the dorso-ventral and the pitching disturbances.

As depicted in Fig. 2, there are two coordinate systems defined in the present study: a global coordinate system (X, Y, Z) with the X-axis horizontal and pointing forward while Z-axis vertical and pointing downward; and a body-fixed coordinate system (x, y, z) with

the origin at the center of mass. Figure 2 shows the state variables which are expressed as the forward (u) and dorso-ventral (w) components of velocity along x- and z-axes, respectively, the pitching angular-velocity (q) around the center of mass, and the pitch angle between the x-axis and the horizontal (θ).

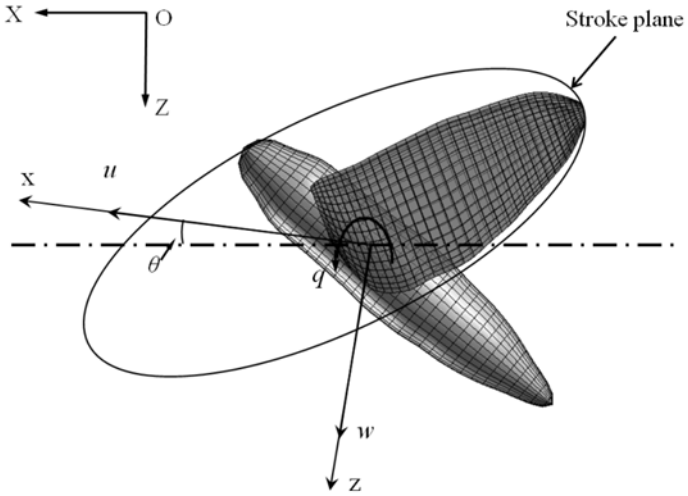

Fig. 2 Definitions of the coordinate systems and the state variables

The equations of motion are intrinsically non-linear, but may be linearized by approximating the body's motion as a series of small disturbances from a steady, symmetric reference flight condition [3, 4]. Then the linearized equations can be rewritten as:

$$\delta\dot{u} = H_u\delta u/m + H_w\delta w/m + H_q\delta q/m - g\delta\theta \tag{5}$$

$$\delta\dot{w} = V_u\delta u/m + Z_w\delta w/m + Z_q\delta q/m \tag{6}$$

$$\delta\dot{q} = M_u\delta u/I_{yy} + M_w\delta w/I_{yy} + M_q\delta q/I_{yy} \tag{7}$$

$$\delta\dot{\theta} = \delta q \tag{8}$$

where H_u, H_w, H_q, V_u, V_w, V_q, M_u, M_w, and M_q are the aerodynamic derivatives (H and V are the x- and z-components of the total aerodynamic forces, respectively, and M is the pitching moment); m is the mass of the insect; $\boldsymbol{g}$ is the gravitational acceleration; I_y is the pitching moment of inertia about y axis; '.' represents differentiation with respect to time (t); the symbol δ denotes a small disturbance quantity. As illustrated in Fig. 2, the longitudinal state vector is composed of the forward velocity component (u), the dorso-ventral velocity component (v), the angular pitch rate at the center of mass (q), and the pitch angle between the x-axis and the X-axis (θ). The latter two parameters are defined to be positive in the nose-up motion.

Then the non-dimensional forms of Eqs (5)~(8) in vector form can be expressed as:

$$\delta\dot{x} = \mathbf{A}\delta x(t) \tag{9}$$

where $\delta x(t)$ denotes the non-dimensional longitudinal state vector of $\{\delta u^+, \delta w^+, \delta q^+, \delta\theta^+\}$. $\mathbf{A}$ is the non-dimensional system matrix defined as:

$$\mathbf{A} = \begin{bmatrix} H_u^+/m^+ & H_w^+/m^+ & H_q^+/m^+ & -g^+ \\ V_u^+/m^+ & V_w^+/m^+ & V_q^+/m^+ & 0 \\ M_u^+/I_{yy}^+ & M_w^+/I_{yy}^+ & M_q^+/I_{yy}^+ & 0 \\ 0 & 0 & 1 & 0 \end{bmatrix} \tag{10}$$

where $H^+ = H/0.5\rho U_{ref}^2 S_t$, $V^+ = V/0.5\rho U_{ref}^2 S_t$, $M^+ = V/0.5\rho U_{ref}^2 S_t c_m$ are the aerodynamic derivatives; U_{ref} is the reference velocity at the wing tip; ρ is the air density (1.225×10^{-3}g cm^2); S_t is the area of two wings; c_m is the mean wing chord length; m^+ is the nondimensional mass, g^+ is the nondimensional gravity acceleration; I_{yy}^+ is the nondimensional pitching moment of inertia about y axis.

Therefore, the complicated longitudinal dynamic flight of a hawkmoth at flapping flight may be eventually treated as a simplified hovering 'rigid body' with only 3 DOF under a series of small disturbance from the steady motion.

2.3 Technique of eigenvalue and eigenvector

Here we describe in detail the technique of eigenvalue and eigenvector as well as their application in the resolution of dynamic flight stability in the hawkmoth hovering. The equations of motion are defined in a manner of $\dot{\varphi}(t) = \mathbf{A}\varphi(t)$, such as:

$$\begin{bmatrix} \delta\dot{u}^+ \\ \delta\dot{w}^+ \\ \delta\dot{q}^+ \\ \delta\dot{\theta}^+ \end{bmatrix} = \mathbf{A} \begin{bmatrix} \delta u^+ \\ \delta w^+ \\ \delta q^+ \\ \delta\theta^+ \end{bmatrix} \tag{11}$$

This is a first-order differential equation and its general form of solutions may be expressed in a form of

$$\varphi(t) = \varphi(0)exp(\mathbf{A}t) \tag{12}$$

where $\varphi(0)$ are the initial disturbance values matrix at $t = 0$. When eigenvalues λ_j of the system matrix **A** are gained, the roots of the equations can be described as:

$$\begin{bmatrix} \delta\dot{u}^+ \\ \delta\dot{w}^+ \\ \delta\dot{q}^+ \\ \delta\dot{\theta}^+ \end{bmatrix} = \mathbf{C}diag(e^{\lambda_1 t}, e^{\lambda_2 t}, e^{\lambda_3 t}, e^{\lambda_4 t})\mathbf{C}^{-1} \begin{bmatrix} \delta u_0 \\ \delta w_0 \\ \delta q_0 \\ \delta\theta_0 \end{bmatrix} \tag{13}$$

Where δu_0, δw_0, δq_0 and $\delta\theta_0$ are the initial disturbance values and **C** is a nonsingular matrix composed of the eigenvectors corresponding to eigenvalues λ_i (i=1, 2, 3, 4).

Here we take the term δu^+ as an example to describe the technique of the eigenvalue and eigenvector. As one of the roots of the linear disturbance equations, the x-component disturbance velocity may be represented by

$$\delta u^+ = \mathbf{C_1}e^{\lambda_1 t} + \mathbf{C_2}e^{\lambda_2 t} + \mathbf{C_3}e^{\lambda_3 t} + \mathbf{C_4}e^{\lambda_4 t} \tag{14}$$

where C_1, C_2, C_3 and C_4 are unique constants depending on the initial values. Therefore the dynamic flight stability based on equation (14) is apparently dependent upon a fact how the initial disturbance values become when time goes by, and a key factor is the sign of the power $\lambda_j t$. To further explain the theory, we assume the 4×4 matrix **A** has a pair of complex eigenvalues and two real eigenvalues, which may be expressed as $\lambda_{1,2} = n_1 + \omega i$, $\lambda_3 = n_2$, and $\lambda_4 = n_3$, respectively. Thus, the x-component motion with the x-component disturbance can be expressed as:

$$\delta u^+ = e^{n_1 t}(\mathbf{C_5}cos\omega t + \mathbf{C_6}sin\omega t) + \mathbf{C_3}e^{n_3 t} + \mathbf{C_4}e^{n_4 t} \tag{15}$$

where the coefficients $\mathbf{C_5} = \mathbf{C_1} + \mathbf{C_2}$ and $\mathbf{C_6} = \mathbf{C_1} - \mathbf{C_2}$ are real numbers. Obviously, if the four eigenvalues are all complex values the mode of motion is identified as an oscillatory one; if they are all real values the mode is a non-oscillatory motion; and if they have both the mode is a linear combination of the oscillatory and non-oscillatory motions. In an oscillatory motion, the angular frequency ω identifies the period of the oscillatory motion which is given as $t_{oscillatory} = 2\pi/\omega$.

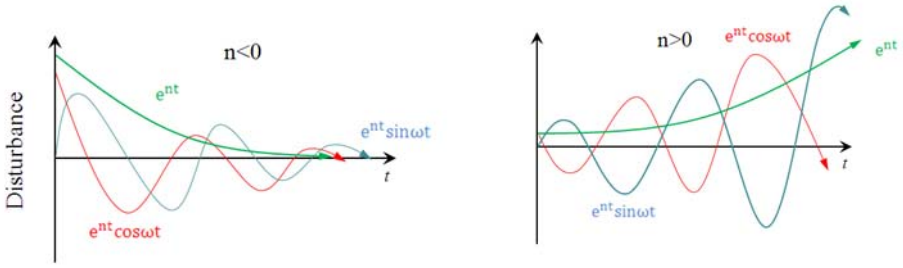

Fig. 3 The variety of disturbance with respect to different eigenvalues when the real part n<0 (A) and n>0 (B).

In this time-varying equation, any variation of the disturbance depends on the sign of the real part of the eigenvalue. If the real part is positive as shown in Fig. 3(A), any time increments result in increasing of disturbance exponentially in a manner of $lim\ \varphi(t) \to \infty$; and the corresponding natural mode is dynamically unstable. Here, for both oscillatory and non-oscillatory motions, we can further quantify its timescale where the initial disturbance is measured to be double, which is given by

$$t_{double} = \mathbf{ln}2/n \tag{16}$$

On the other hand, if the real part is negative as shown in Fig. 3(B), any time increments, however, lead to exponential decrease and decay of the initial disturbance and hence $lim\ \varphi(t) = 0$; and the corresponding natural mode is dynamically stable. A timescale for halfing the starting values is given by

$$t_{half} = \mathbf{ln}2/|n| \tag{17}$$

Accordingly, a real natural mode of a hawkmoth is, in principal, based on a linear combination of the modes corresponding with each eigenvalue. Therefore, we can examine each mode corresponding with each eigenvalue in a separated manner.

2.4 The equilibrium condition

The equilibrium condition for hovering flight is determined as the reference flight condition in the present study. A hovering mode is described as that the mean wing force is exactly vertical and precisely balances the weight of the insect without producing any body movement and rotation. More strictly speaking, the hovering mode can merely be realized when the mean horizontal force equals to zero and the mean vertical force just supports the weight of the insect while the mean pitching moment vanishes. Since the CFD-based simulation of hovering flight normally outputs somehow non-zero three aerodynamic forces and moments even though realistic morphological and kinematic models are used we need to seek an equilibrium condition through adjusting the kinematic parameters in terms of the stroke plane angle and the angle of attack of the flapping wing.

The weight of an insect can be non-dimensionalized as $G^+ = mg/0.5\rho U_{ref}^2 S_w$, where mg is the weight of the insect; and S_w is the surface area of a single wing. For a hawkmoth with a weight of approximately 1.5g, i.e., mg = 7.8 mN, U_{ref} =5.06 ms^{-1} and S_w = 9.6 cm^2. So the

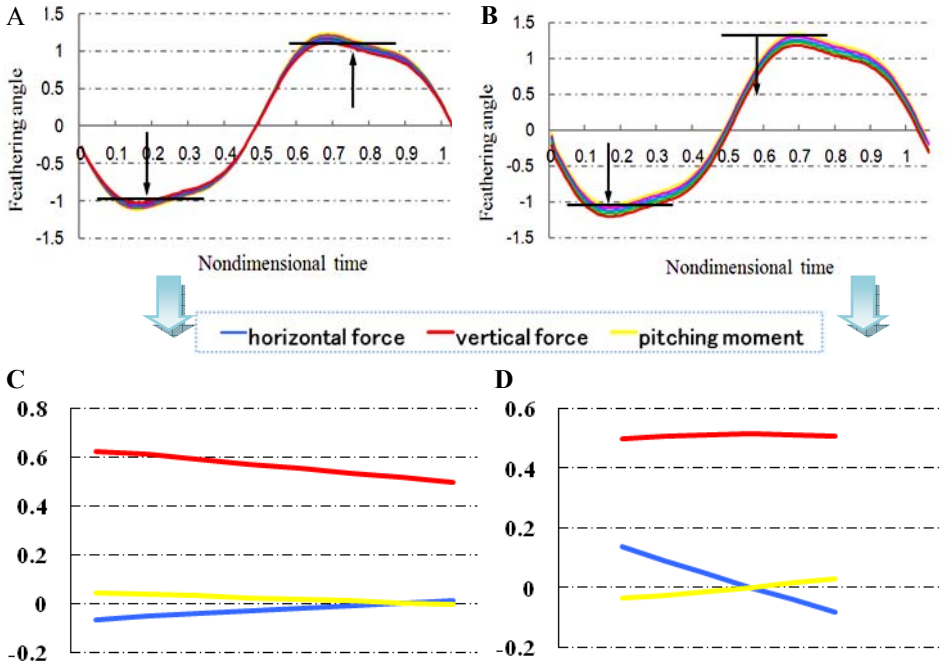

Fig.4 (A) Increase the absolute value of feathering angle (B) Shift the feathering angle downward. (C) The corresponding mean forces and moment when increase the absolute value of feathering angle and (D) shift the feathering angle downward. The horizontal axes of (C) and (D) express the different cases when changing the feathering angle above, respectively.

non-dimensional weight G^+ is calculated to be 1.04, which corresponds with a mean vertical force coefficient of the same magnitude.

On a basis of the kinematic data of a hovering hawkmoth, *Manduca* by Willmott and Ellington[9], we used the following kinematic parameters in our study: a body angle $\chi = 39.8$ *degree*, a stroke plane angle $\beta = 15$ *degree*, a flapping amplitude Φ=114.4 *degree*, a mean wing chord length c_m =1.83 cm, a wing length $R = 4.83$ cm, and a wingbeat frequency $f = 26.1\ s^{-1}$. Accordingly, the Reynolds number is defined by $Re = c_m U_{ref}/\nu$ and is calculated to be 6300 whereas the reduced frequency K is 0.298.

The angle of attack of the wing plays a key role in the aerodynamic force generation during flapping flight and therefore it is an important issue to appropriately adjust the time-varying angle of attacks so as to accomplish the exactly balanced equilibrium condition. The realistic kinematics, in particular the time-varying feathering angles measured by Willmott and Ellington[9], however, are not exactly equal to the angles of attack when the elevation angle is not equal to zero. As the feathering angle shows distinguished variation along the spanwise of the flapping wing they thereby measured a series of feathering angles spanwise from $0.3R$ to $0.9R$ with an interval of $0.1R$, and calculated a mean angle of attack accordingly.

To tune the feathering angles or the angles of attack for the equilibrium condition, we use two methods as illustrated in Fig. 4. One is by increasing the absolute value or the amplitude of the feathering angle during a complete cycle (Fig.4A). The resulted variations of mean aerodynamic forces and moment are plotted below correspondingly (Fig.4C). The other is by shifting the feathering angle downward (Fig.4B) and the corresponding mean aerodynamic force and moment are shown below (Fig.4D). Based on the fact that the vertical force shows slight change in the latter case, we first utilize the former one to determine the mean feathering angle (i.e., the amplitude) to seek a temporal equilibrium state where the vertical force equal to 5.17. Then the latter method is applied to satisfy the condition that the horizontal force vanishes while the pitching moment also reaches zero through a process of trial and error by tuning the shifting of the feathering angle. When the time course of the feathering angle during a complete beating cycle is determined, we then have all the dynamic parameters for the equilibrium condition.

2.5 Aerodynamic derivatives

As stated above, the disturbance from outside that the insect undergoes is treated as the relative motion of the insect from a reference flight condition (hovering flight). And the three components of the disturbance, namely, the elevation in x-and z-axis and the pitching movement can be transformed to a x-component of velocity u, a z-component of velocity w and a pitching angular velocity q about the center of mass, respectively. In order to estimate the aerodynamic derivatives, we consider three disturbance conditions for the three state variables (u, w, q) separately. For instance, when the dimensionless x-component of velocity u^+ is considered to vary in a range while z-component of velocity w and the pitching angular velocity q are fixed to be zero; and this disturbance condition is called the u-series. Similar procedures are also applied for the w-series and the q-series.

The aerodynamic forces and moments are then computed under the equilibrium condition with consideration of the three disturbances. In calculating the aerodynamic derivatives under each disturbance condition, we subtract the aerodynamic forces and moment of the equilibrium state from those with the disturbance to obtain the difference between the equilibrium and disturbed conditions. Then, with the range of consecutive small disturbances as the abscissa and the corresponding difference in aerodynamic forces and moments as the ordinate, a set of curves are plotted for the three disturbance conditions. And the local tangents of the curves are calculated to be the three aerodynamic derivatives.

3. Results

3.1 Aerodynamic forces and moment

As shown in Fig. 5(A), Fig. 6(A) and Fig. 7(A), the disturbances of x- and z-components of velocity and pitching angular velocity vary in a range of -0.1~0.1(-0.5~0.5 ms^{-1}) with an interval of 0.01. The vertical axis shows the difference between the disturbance and equilibrium. Obviously, all the three curves show approximately linear variation. Accordingly the aerodynamic derivatives, H_u^+, V_u^+, M_u^+, H_w^+, V_w^+, M_w^+, H_q^+, V_q^+, and M_q^+ can be calculated by taking the local tangents of the curves as given in Table 1.

Table 1 Non-dimensional aerodynamic derivatives$^+$

H_u^+	V_u^+	M_u^+	H_w^+	V_w^+	M_w^+	H_q^+	V_q^+	M_q^+
-1.33	0.059	1.89	0.23	-1.52	0.17	-0.67	-0.13	-0.17

Next we give a comprehensive discussion on relationship between the three disturbance conditions and their influences on aerodynamic forces and moments. With consideration of the u-series, when $\Delta u^+ > 0$ (where the insect moves forward), the x-component of force decreases while the pitching moment increases with increasing of the disturbance velocity u, and vice versus when $\Delta u^+ < 0$. Note that the z-component of force has slight change with respect to the forward motion compared with the x-component of force and the pitching moment, which results in relatively large H_u^+ and M_u^+ but small V_u^+. Furthermore, the monotonic ascending pitching moment as in Fig. 5(A) implies that a nose-up or nose-down pitching moment may be observed when the insect moves forward or backward. Fig. 5(B) shows the variation in aerodynamic forces and moments during a complete flapping cycle at $\Delta u^+ = 0.06$. During the downstroke, with the forward velocity Δu^+, the wing shows a larger velocity than that in the reference flight, which results in larger lift and drag forces. During the upstroke, however, a relatively smaller velocity leads to decreasing of the lift but increasing of the drag.

The w-series as in Fig. 6(A) shows slight variation in the x-component of force and the pitching moment but an apparent decrease in the z-component of force. This implies that, compared with the u-series, the pitching moment in the w-series is hardly produced when insect moves downward or upward; and hence we observe relatively large V_w^+ but small H_w^+ and M_w^+. Fig. 6(B) shows the variation of aerodynamic forces and moment at $\Delta w^+ = 0.06$. At downstroke, the flapping wing is considered to have a larger downward velocity and thus results in an increase in lift and drag forces and pitching moment. At upstroke, however, both drag and pitching moment turn to decrease slightly.

With regarding to the q-series, obviously the changes in three state variables are a margin, in particular in the z-component of force and the pitching moment. Note that, as a resultant of x- and z-components of motions, the body of hawkmoth rotates about the center of mass but the effect is very subtle compared with the x- and/or z-components of disturbances. As seen in Fig. 7(B), based on the changes in a wing-beat cycle at $\Delta q^+ = 0.06$, we note that the changes in state variables in the q-series can be considered as a combination of the u- and w-series. Furthermore, when the body starts to pitch about the body angle of 39.8 degree, the x-and z-components of velocity are almost even.

3.2 The eigenvalues and eigenvectors

Based on the computed aerodynamic derivatives, we can construct the system matrix and obtain the eigenvalues and eigenvectors. As shown in Table 2 and 3, four eigenvalues $\lambda_{1,2}$, λ_3 and λ_4 yield with a pair of complex $\lambda_{1,2}$ which have a common negative real part and two opposite imagine values. As described in the previous section, these four eigenvalues represent three natural modes: a stable oscillatory motion and two subsidence modes. Furthermore, the polar form of the eigenvectors can be expressed as displayed in Table 4. Since eigenvectors are unique in direction but not in magnitude we have scaled them to make $\delta\theta = 1$.

To distinguish the two subsidence modes, a timescale is hereby introduced to measure the time being required for halving or doubling the initial disturbance values. With the Eq. (17) the timescales of the two modes are calculated to be $t^+_{\text{half}} = 0.9$ and $t^+_{\text{half}} = 3.2$, respectively, which point to a fast subsidence mode and a slow subsidence mode, respectively. Note that here we don't term them the so-called 'short period mode' or 'long period mode' as normally used in the stability study of aircraft simply because they are of non-oscillatory modes.

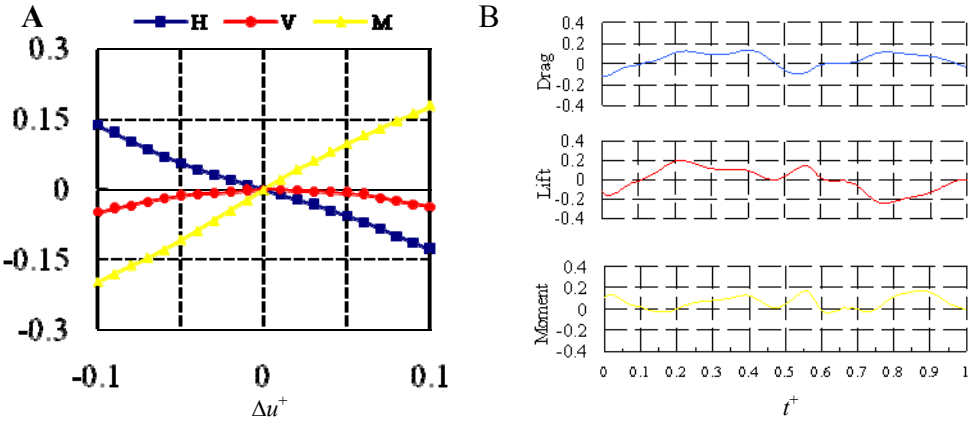

Fig.5 (A) x-component and z-component of forces and pitching moment when the x-component of velocity u varies in a range of -0.1~0.1. (B) Time course of the differences in lift, drag and pitching moment with respect to the reference flight condition at $\Delta u^+ = 0.06$. t^+ is a dimensionless time

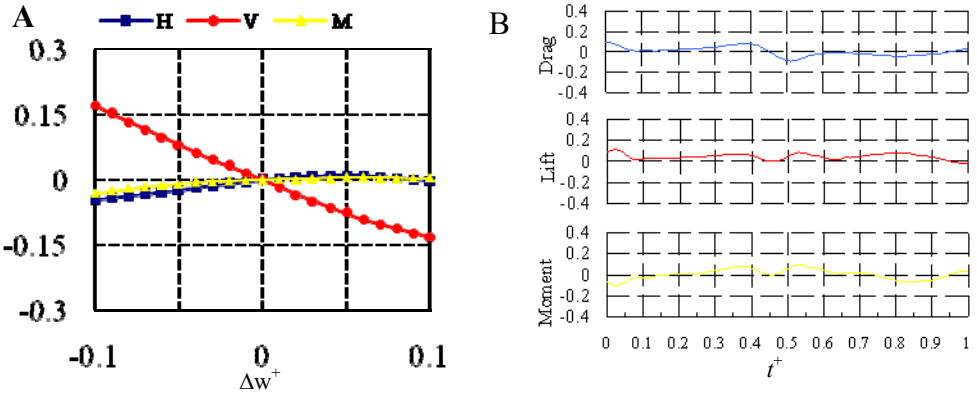

Fig. 6 (A) x-component and z-component of forces and pitching moment when the z-component velocity w varies in a range of -0.1~0.1. (B) Time course of the differences in lift, drag and pitching moment with respect to the reference flight condition at $\Delta w^+ = 0.06$. t^+ is a

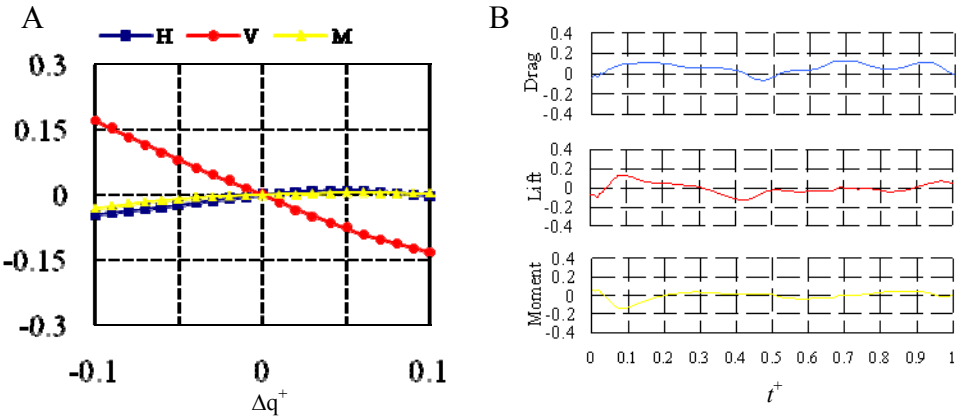

Fig. 7 (A) x-component and z-component of forces and pitching moment when the pitching angular velocity q varies in a range of -0.1~0.1. (B) Time course of the differences in lift, drag and pitching moment with respect to the reference flight condition at $\Delta q^+ = 0.06$. t^+ is a dimensionless time

Table 2 Eigenvalues of the system matrix

Mode 1 ($\lambda_{1,2}$)	Mode 2 (λ_3)	Mode 3 (λ_4)
-0.116±0.927i	-0.78	-0.216

Table 3 Eigenvectors of the system matrix

	Mode 1	Mode 2	Mode 3
δu^+	0.074±0.04i	0	-0.085
δw^+	0.013±0.002i	0.02	0.862
δq^+	0.085±0.675i	0.615	-0.105
$\delta\theta^+$	-0.728±5.46×$10^{-5}i$	-0.788	0.488

4. Discussion

4.1 The stable oscillatory mode

As shown in Fig. 8, the pair of conjugated complex eigenvalues represents a stable oscillatory mode. A nondimensionalized period of the oscillatory mode is computed to be approximately $t^+_{oscillatory}$= 6.8, which is a relative short period. As the reference time used in the non-dimensionalization of motion is the wingbeat period, this oscillatory has a period of 6.8 times of the wingbeat period. In addition, the time being taken to half the disturbance values is computed to be t^+_{half} =6, which indicates that the insect takes approximately six wingbeats to half the initial disturbance values.

Furthermore, it is interesting to find in Table 4 that the variation in the z-component of velocity (δw^+) is a margin and can be negligible in the oscillatory mode compared with the x-component of velocity (δu^+) and pitching angular velocity (δq^+). This implies that in the oscillatory mode the hawkmoth shows some kinds of x-component and pitching oscillations. In addition, it is seen that based on the computed phase angles both δu^+ and δq^+ are out of phase with $\delta\theta^+$. That indicates that a positive initial pitching angle of a hovering hawkmoth accompany with a negative x-component of velocity and a negative pitching angular velocity. Therefore, the hovering hawkmoth in this mode performs a horizontal movement with a nose-up pitching rotation.

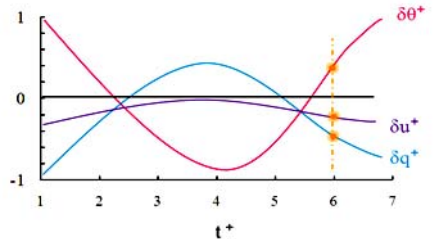

Fig. 8 Disturbance δu^+, δq^+, and $\delta\theta^+$ in the stable oscillatory mode

4.2 The fast subsidence mode

A relatively large real eigenvalue identifies a fast subsidence mode as shown in Fig. 9. In this mode, the time being taken to halve the initial disturbance value is computed to be t^+_{half} =0.9, which means that the hawkmoth merely spends approximately one wingbeat with its disturbance damped out to a half.

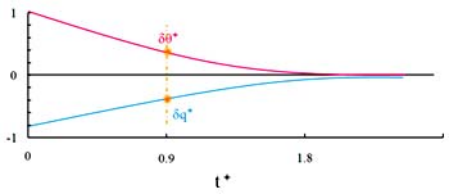

Fig. 9 Disturbance δq^+ and $\delta\theta^+$ in the stable fast subsidence mode.

In this mode as shown in Table 4, the pitch rate is obviously a leading factor with one order greater than the other state variables. The δq^+ is out of phase with $\delta\theta^+$, which implies that a positive initial $\delta\theta^+$ will lead to a negative δq^+, pointing to a nose-down pitching motion. Therefore, the natural motion of the hawkmoth would be a pitching rotation but in an opposite direction compared with the initial pitch-attitude $\delta\theta^+$.

4.3 The slow subsidence mode

A relatively small real eigenvalue identifies a slow subsidence mode as shown in Fig. 10.

In this mode, the time taken to halve the starting disturbance value is computed to be $t^+_{half} = 3.2$, which means that the hawkmoth will halve the starting disturbance value in approximately three wingbeats. The eigenvectors show that δw^+ shows much larger magnitude than the other state variables. However, δq^+ and δu^+ are still not small enough to be negligible in comparison with the previous two modes. Furthermore, it is obvious that both δu^+ and δq^+ are out of phase with the pitch-attitude whereas δw^+ and $\delta\theta^+$ are in phase. That indicates that a positive initial pitch angle for a hovering hawkmoth would result in a positive δw^+ but negative δu^+ and δq^+, which point to that the insect ascends with a nose-down pitching and a slight backward moving.

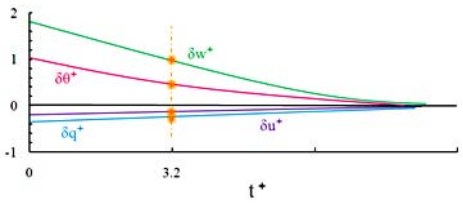

Fig. 10 Disturbance δu^+, δw^+, δq^+, and $\delta\theta^+$ in the stable slow subsidence mode.

Table 4 Magnitudes and phase angles of each of three eigenvectors

Mode	δu^+	phase angle	δw^+	phase angle	δq^+	phase angle	$\delta\theta$	phase angle
Stable oscillatory	0.118	180°	0.018	180°	0.935	180°	1	0°
Fast subsidence	0	180°	0.025	180°	0.78	180°	1	0°
Slow subsidence	0.174	180°	1.766	0°	0.215	180°	1	0°

4.4 The inherent dynamical stability

The inherent dynamical stability has been analyzed initially by Taylor and Thomas[3] in studying the dynamic stability of a desert locust and furthermore by Sun and Xiong[4] in studying the dynamical stability of a bumblebee. The conclusions reached in their studies can be clarified as: (1) a desert locust is identified with three natural longitudinal modes of motion involving one stable oscillatory mode, one stable subsidence mode and one unstable divergence mode; and (2) a bumblebee is identified with three natural longitudinal modes of motion containing one unstable oscillatory mode, one stable fast subsidence mode and one stable slow subsidence mode. A common conclusion in the two studies states that one unstable mode of the three motion modes may exist in the dynamic flight stability of the two insects. In the present study, however, all the three natural modes of a hawkmoth are dynamically stable. With consideration of the similarity of using the CFD methods in the dynamic flight stability analysis we make an extended discussion on the difference between our results and those by Sun and Xiong[4]. We notice that, even though a similar methodology on simplifying the equations of motion and the technique of eigenvalues and eigenvectors is utilized a key difference in the CFD-based modeling of the problem is that we employ a set realistic kinematics for both the flapping wing and the body. However, Sun and Xiong[4] used the idealized time course of symmetrically flapping wing kinematics by Dickinson, et al.[10] but without considering the realistic data neither of the stroke plane angle nor the body angle. We also notice that their results show an unstable oscillatory mode but with a very small positive real part. We believe that the equilibrium condition and the resulted aerodynamic derivatives may be very sensitive to any changes in the wing kinematics and utilization of realistic kinematics should be a must and a starting point. No doubt further extended studies on the effects of wing kinematics and size and morphology need to be done.

We further make an extended analysis on how the natural mode affects the disturbances. According to the principle of a linear superposition, and in the absence of any control inputs

beyond the system matrices, the natural flight behavior of a hawkmoth may be considered as a sum of these modes. Thus, the natural mode of a hawkmoth is composed of three modes involving a stable oscillatory mode, a stable fast subsidence mode and a stable slow subsidence mode. Since our results show that the three modes are all stable, the resultant natural mode must be stable either. Though the resultant mode is of complicated forms, the general attitude can be described qualitatively as below.

Here we take the x-component of disturbance as an example. By substituting the eigenvalues into the Eq. (15) we can have the following expression, such as:

$$\delta u^{+} = e^{-0.12t}(\mathbf{C}_5 cos0.927t + \mathbf{C}_6 sin0.927t) + \mathbf{C}_3 e^{-0.78t} + \mathbf{C}_4 e^{-0.22t} \quad (18)$$

Clearly, in the natural mode of a hawkmoth, an oscillatory attitude shows an exponentially decreasing tendency with increasing of time; the period of the oscillatory model is obviously the same as that computed in the section 4.1, $t_{\text{oscillatory}} = 2\pi/\omega = 6.8$.While the initial value of the disturbance is unknown here and hence it is difficult to determine a precise timescale for the disturbance damping, this no doubt points to a fact that this natural mode is a dynamically stable one.

5. Conclusion

In the present study, a computational study of dynamic flight stability of hovering hawkmoth is conducted using an insect dynamic flight simulator and the technique of eigenvalues and eigenvectors with consideration of realistic morphology and kinematics. The longitudinal dynamical stability of a hawkmoth in hovering is investigated, which demonstrates that the hovering hawkmoth is very likely inherent dynamically stable even in an absence of any active controls. This implies that the hovering hawkmoth may not need to adjust their wing motions under any small disturbance condition and hence could return to the equilibrium state 'automatically'.

Acknowledgements

The present work was partly supported by a PRESTO/JST (Japan Science and Technology Agency), entitled of A Biology-inspired Dynamic Flight Simulator, and the Grant-in-Aid for Scientific Research of No. 18656056 and No. 18100002. The computations were performed on the RIKEN Super Computer (RSCC).

References

(1) Thomas, A. L. R. and Taylor, G. K., Animal Flight Dynamics. I. Stability in Gliding Flight, *J. Theor. Biol.* Vol.212, (2001), pp.399-424.
(2) Taylor, G. K. and Thomas, A. L. R., Animal Flight Dynamics. II. Longitudinal Stability in Flapping Flight, *J. Theor. Biol*. Vol.214, (2002), pp.351-370.
(3) Taylor, G. K. and Thomas, A. L. R., Dynamic Flight Stability in the Desert Locust *Schistocerca gregari*, *J. Exp. Biol*. Vol.206, (2003), pp.2803-2829.
(4) Sun, M. and Xiong, Y., Dynamic Flight Stability of a Hovering Bumblebee, *J. Exp. Biol.* Vol.208, (2005), pp.447-459.
(5) Liu, H. and Kawachi, K., A Numerical Study of Insect Flight, *J. Comp. Phys.*, Vol.146, (1998), pp.124-156.
(6) Liu, H, Simulation-Based Biological Fluid Dynamics in Animal Locomotion, *Trans. ASME*, *Appl. Mech. Rev.*, Vol.58, no.4 (2005), pp.269-282.
(7) Aono, H. and Liu, H., Vortical structure and aerodynamics of Hawkmoth hovering, *J. Biom. Sci. and Eng*. Vol. 1, No.1, (2006), pp.234-245.
(8) Aono, H. Liang F. Y. and Liu, H., Near- and far-field aerodynamics in insect hovering flight: an integrated computational study, *J. Exp. Biol.* (2007), to appear
(9) Willmott, A. P. and Ellington, C. P., The Mechanics of Flight in the Hawkmoth *Manduca Sexta*. I. Kinematics of Hovering and Forward Flight, *J. Exp. Biol.* Vol.200, (1997), pp.2705-2722.
(10) Dickinson, M. Lehmann, F.-O., and Sane, S. P., Wing Rotation and the Aerodynamic Basis of Insect Flight, *Science*, Vol.284, (1999), pp.1954-1960.